

Accelerated Article Preview

Evolutionary and biomedical insights from a marmoset diploid genome assembly

Received: 20 September 2020

Accepted: 12 April 2021

Accelerated Article Preview Published
online 28 April 2021

Cite this article as: Yang, C. et al.
Evolutionary and biomedical insights from
a marmoset diploid genome assembly.
Nature <https://doi.org/10.1038/s41586-021-03535-x> (2021).

Open access

Chentao Yang, Yang Zhou, Stephanie Marcus, Giulio Formenti, Lucie A. Bergeron, Zhenzhen Song, Xupeng Bi, Juraj Bergman, Marjolaine Marie C. Roussele, Chengran Zhou, Long Zhou, Yuan Deng, Miaoquan Fang, Duo Xie, Yuanzhen Zhu, Shangjin Tan, Jacquelyn Mountcastle, Bettina Haase, Jennifer Balacco, Jonathan Wood, William Chow, Arang Rhie, Martin Pippel, Margaret M. Fabiszak, Sergey Koren, Olivier Fedrigo, Winrich A. Freiwald, Kerstin Howe, Huanming Yang, Adam M. Phillippy, Mikkel Heide Schierup, Erich D. Jarvis & Guojie Zhang

This is a PDF file of a peer-reviewed paper that has been accepted for publication. Although unedited, the content has been subjected to preliminary formatting. Nature is providing this early version of the typeset paper as a service to our authors and readers. The text and figures will undergo copyediting and a proof review before the paper is published in its final form. Please note that during the production process errors may be discovered which could affect the content, and all legal disclaimers apply.

Evolutionary and biomedical insights from a marmoset diploid genome assembly

<https://doi.org/10.1038/s41586-021-03535-x>

Received: 20 September 2020

Accepted: 12 April 2021

Published online: 28 April 2021

Open access

Chentao Yang^{1,2,19}, Yang Zhou^{1,19}, Stephanie Marcus^{3,19}, Giulio Formenti^{3,4}, Lucie A. Bergeron², Zhenzhen Song⁵, Xupeng Bi¹, Juraj Bergman⁶, Marjolaine Marie C. Rousselle⁶, Chengran Zhou¹, Long Zhou¹, Yuan Deng^{1,2}, Miaoquan Fang¹, Duo Xie¹, Yuanzhen Zhu¹, Shangjin Tan¹, Jacquelyn Mountcastle⁴, Bettina Haase⁴, Jennifer Balacco⁴, Jonathan Wood⁷, William Chow⁷, Arang Rhie⁸, Martin Pippel^{9,10}, Margaret M. Fabiszak¹¹, Sergey Koren⁸, Olivier Fedrigo⁴, Winrich A. Freiwald^{11,12}, Kerstin Howe⁷, Huanming Yang^{1,5,13,14}, Adam M. Phillippy⁸, Mikkel Heide Schierup⁶, Erich D. Jarvis^{3,4,15} & Guojie Zhang^{2,16,17,18} ✉

The accurate and complete assembly of both haplotype sequences of a diploid organism is essential to understanding the role of variation in genome functions, phenotypes, and diseases¹. Here, using a trio-binning approach, we present a high-quality, diploid reference genome, with both haplotypes assembled independently at the chromosome level, for the common marmoset (*Callithrix jacchus*), an important primate model system widely used in biomedical research^{2,3}. The full heterozygosity spectrum between the two haplotypes involves 1.36% of the genome, much higher than the 0.13% indicated by the standard single nucleotide heterozygosity estimation alone. The *de novo* mutation rate is 0.43×10^{-8} per site per generation, where the paternal inherited genome acquired twice as many mutations as the maternal. Our diploid assembly enabled us to discover a recent expansion of the sex differentiated region and unique evolutionary changes in the marmoset Y chromosome. Additionally, we identified many genes with signatures of positive selection that might have contributed to the evolution of *Callithrix* biological features. Brain related genes were highly conserved between marmosets and humans, though several genes experienced lineage-specific copy number variations or diversifying selection, providing important implications for the application of marmosets as a model system.

A diploid organism carries two haploid genomes with a range of variants, which make significant contributions to phenotypic variations⁴. Phased haplotype assemblies can help to reveal the cis- and trans-acting variants on the two homologous genomes. However, most contemporary *de novo* genome sequencing efforts produce a single mosaic reference genome derived from parts of both maternal and paternal alleles, where variations between homologous chromosomes are normally disregarded. As a consequence, these methods usually fail to assemble genomic regions with high heterogeneity, resulting in fragmented sequences. A few methods have been developed to produce partial haplotype-phased genome assemblies and showed power in using long sequencing reads to produce long haplotigs (haplotype-specific contigs)^{5,6}. However, producing an assembly completely phased at the chromosome level for both haplotypes of a diploid genome remains

a challenge. Here, as part of the Vertebrate Genomes Project, we applied a trio-binning approach^{7,8} to produce a chromosome-level, fully haplotype-resolved diploid genome assembly for the common marmoset, *Callithrix jacchus*. This New World primate has been established as an animal model for a broad range of biomedical research such as neuroscience, stem cell biology, and regenerative medicine^{2,3}. With our high-quality diploid assembly, we discovered novel properties of heterozygosity on both autosomes and sex chromosomes of this primate species.

Diploid genome assembly

We generated 63x coverage PacBio continuous long reads, 55x 10X Genomics chromium linked-reads, 154x Bionano optical molecules,

¹BGI-Shenzhen, Shenzhen, 518083, China. ²Villum Centre for Biodiversity Genomics, Section for Ecology and Evolution, Department of Biology, University of Copenhagen, DK-2100, Copenhagen, Denmark. ³Laboratory of Neurogenetics of Language, The Rockefeller University, 1230 York Ave, New York, NY, 10065, USA. ⁴Vertebrate Genome Lab, The Rockefeller University, New York City, NY, USA. ⁵University of the Chinese Academy of Sciences, Beijing, 100049, China. ⁶Bioinformatics Research Centre, Aarhus University, DK-8000, Aarhus C, Denmark. ⁷Wellcome Sanger Institute, Hinxton, UK. ⁸Genome Informatics Section, Computational and Statistical Genomics Branch, National Human Genome Research Institute, National Institutes of Health, Bethesda, MD, USA. ⁹Max Planck Institute of Molecular Cell Biology and Genetics, Dresden, Germany. ¹⁰Center for Systems Biology, Dresden, Germany. ¹¹Laboratory of Neural Systems, The Rockefeller University, 1230 York Ave, New York, NY, 10065, USA. ¹²Center for Brains, Minds and Machines (CBMM), Rockefeller University, New York, NY, USA. ¹³James D. Watson Institute of Genome Sciences, 310058, Hangzhou, China. ¹⁴Guangdong Provincial Academician Workstation of BGI Synthetic Genomics, BGI-Shenzhen, Shenzhen, 518120, China. ¹⁵Howard Hughes Medical Institute, Chevy Chase, MD, USA. ¹⁶State Key Laboratory of Genetic Resources and Evolution, Kunming Institute of Zoology, Chinese Academy of Sciences, 650223, Kunming, China. ¹⁷China National GeneBank, BGI-Shenzhen, Shenzhen, 518120, China. ¹⁸Center for Excellence in Animal Evolution and Genetics, Chinese Academy of Sciences, 650223, Kunming, China. ¹⁹These authors contributed equally: Chentao Yang, Yang Zhou, Stephanie Marcus. ✉e-mail: guojie.zhang@bio.ku.dk

105x Hi-C reads from a male F1 marmoset, and 70x short read sequences from the DNA of both parents (Supplementary Table 1 and Supplementary Fig. 1). We used an updated version of TrioCanu⁷⁸ to bin the F1's PacBio long reads via k-mers of the parental short reads, and assembled each set into haploid-specific contigs, which were independently scaffolded with the 10X, Bionano, and Hi-C data⁸ (Extended Data Fig. 1, Supplementary Fig. 2, Supplementary Tables 2, 3). The final contig and scaffold NG50s after manual curation were 7.7 Mb and 146 Mb for the maternal assembly and 12.1 Mb and 136 Mb for the paternal assembly, respectively. K-mer assessment indicated the assemblies were fully phased (Extended Data Fig. 2a and Supplementary Figs. 3, 4). Each haploid genome includes 22 autosomes and each of the two sex chromosomes (X/Y), with 99.45% and 98.94% of the maternal and paternal alleles assigned to chromosomes, respectively. The assembled chromosome lengths showed clear linear correlation with the estimated marmoset karyotype lengths^{8,9} (Extended Data Fig. 2b, Supplementary Note, Supplementary Tables 4, 5, and Supplementary Fig. 5). Although marmosets show prevalent genetic chimerism between twins and triplets in utero¹⁰, the chimeric level of F1 male muscle sample used in this study was very low, as expected¹¹ (Extended Data Fig. 1d-g, Supplementary Fig. 6, Supplementary Table 6, 7 and Supplementary Note).

We estimated the single-base-pair accuracy rate to be 99.996% for the maternal assembly and 99.998% for the paternal assembly (Supplementary Note, Supplementary Fig. 7 and Supplementary Tables 8, 9). About 93% and 88% of the gaps in the previously published marmoset reference genome cj3.2¹² were closed in our maternal and paternal assemblies, respectively, and both showed over 290-fold increase in contig N50, with 95.75% and 93.62% of the contigs over 1 Mb, respectively (Extended Data Fig. 2c). Iso-Seq full-length transcriptome data also suggest a high completeness of our assembly (Supplementary Note, Supplementary Tables 10, 11). Comparison with two other chromosome-level assemblies recently released (cj1700 and cj2019) show 16 large intra-chromosome-level structural variations (SVs) (>1 Mb) and 3 inter-chromosomal SVs (Supplementary Tables 12, 13). PacBio long reads and 10X linked-reads confirmed our assemblies were correct (Supplementary Figs. 8, 9 and Supplementary Tables 12-14). However, these differences may also be due to the large-structural polymorphisms.

Heterozygosity between parental genomes

In traditional genome sequencing efforts, heterozygosity is normally estimated by mapping sequencing reads onto a mosaic reference genome, resulting in limited phase information of the heterozygous variants. Our assemblies allow us to directly compare the two parentally inherited genomes and identify the full spectrum of genetic variants between the parental alleles, including single nucleotide variations (SNVs), insertion/deletions (indels), and large SVs (Supplementary Fig. 10). We identified 3.47 million SNVs and ~232,000 short (≤ 50 bp) indels across the whole genome (Fig. 1a), with 96.5% SNVs confirmed by short read mapping. PCR experiments validated 99.6% and 95.2% randomly selected SNVs and short indels (Supplementary Notes, Supplementary Tables 15-17), indicating that our diploid assembly allowed us to detect allelic variants with considerably high accuracy. We found a correlation between SNV rate and indel rate (Supplementary Fig. 11a), where both displayed a unimodal distribution across the genomes (Supplementary Figs. 11b, 12). Consistent with laboratory inbreeding, we observed 28 genomic regions with long runs of homozygosity (Fig. 2a), with longest one spanning over 10Mb (Supplementary Fig. 13a). This pattern can also be detected in other marmoset samples with short read resequencing data¹³ (Supplementary Fig. 13b and Supplementary Table 18), suggesting the captive marmosets are suffering significant reduction of genetic diversity.

Heterozygous variations in regulatory or coding regions could result in allele-specific expression profiles or different products of

the same genes from the two alleles¹⁴. We found approximately 1.1% of SNVs and 0.58% of indels were located in protein-coding genes or regulatory regions. In particular, 8,144 SNVs caused non-synonymous substitutions and 274 indels caused frame-shifting mutations, which can produce allele-specific transcripts and proteins. This observation was validated by the Iso-Seq data, where we detected that 2,537 genes produced transcripts with variation in open-reading frames from the parental alleles (Supplementary Fig. 14).

SVs contribute substantial genetic diversity with important evolutionary and medical implications. By comparing the two haploid genomes, we identified 11,663 SVs (>50 bp), including 6,064 large indels, 27 inversions, 34 translocations, 5,514 copy number variations (CNVs), and 24 inverted translocations (Fig. 2a and Supplementary Table 19). We validated 95.7% of large indels and 74.2% of SVs with PacBio long reads, as well as 14 of 17 randomly selected large indels by PCR (Supplementary Fig. 15 and Supplementary Table 20). By counting all types of variations between the two haploid genomes, we estimate the overall heterozygosity rate on the autosomes of the sequenced individual to be ~1.36%.

Large heterogeneous SVs could cause a high incidence of chromosomally unbalanced gametes and thus are normally rare¹⁵. We found that 72% of SVs were shorter than 1.5 kb, with an average length of about 3.5 kb. The longest SV was a 304 kb inversion (Supplementary Fig. 16). We observed a higher density of LINE/L1 around the inversions ($p = 0.0078$, one-sided t-test), which peaked at a length of 300 bp and were enriched with Alu repeats (Supplementary Fig. 17a; $p = 2.2e-16$, Chi-squared test, Supplementary Note). About 33% of inversion variations between haplotypes were located between two inverted repeat sequences (Supplementary Fig. 17b), indicating they were introduced by a repeat mechanism¹⁶. We detected and validated 58 genomic translocation events that differed between the two haplotypes including 50 genes (Fig. 2a and Supplementary Table 21). About half of the affected genes were completely translocated from one allele to a different genomic location in the other allele. The mechanism driving such translocations still needs to be elucidated.

De novo germline mutations

Germline mutations are the source of genetic diversity and the driving force of both evolution and genetic diseases¹⁷. Yet, finding *de novo* germline mutations is still a challenging task, where in traditional assemblies less than half of the mutations can be phased to parental origin¹⁸. A fully diploid assembly allows us to use each parental haplotype independently as a reference to detect *de novo* mutations, and validate the loci detected independently from the two references as controls for false-positive calls (see Methods and Supplementary Note). We detected 9 validated *de novo* mutations in this trio from the ~41% of callable sites in both maternal and paternal genomes (Fig. 1a, triangles and Supplementary Table 22). The paternal-to-maternal ratio contribution of *de novo* mutations to the child was 2:1 (Fig. 1b), which is lower than that in humans (4:1)¹⁸ but similar to the closely related owl monkey (2.1:1)¹⁹. Our results suggest a mutation rate of 0.43×10^{-8} *de novo* mutations per site per generation for the marmoset. Using this new estimated rate and the evolutionary branch length of marmoset substitutions inferred from whole-genome alignments²⁰, we estimated a divergence time between New World Monkeys (NWMs) and humans at ~48.7 million years ago (Mya), which is close to what was estimated from the owl monkey¹⁹.

Marmoset new sex differentiation region

Based on sequencing depth of parental short reads on the F1 male assembly (see Methods), we identified ~147 Mb X-linked sequences with over 99% in a single X chromosome scaffold (Supplementary Table 23). Since the Y chromosome is enriched with repeat elements

and segmental duplications, we decollapsed unplaced and potential Y-linked scaffolds²¹ (Supplementary Fig. 18a) then combined read depth information and Hi-C interactions to identify 13.85 Mb final Y-linked sequences (Supplementary Fig. 18b, Supplementary Table 24, see Methods). This is smaller yet closer to the 20 Mb karyotype estimate⁹ and longer than that in other assemblies (Supplementary Table 25).

Our diploid assembly resolved pseudoautosomal regions (PARs) of both X and Y, while most other male genomes result in collapsing PARs into one copy with mixed origin. This permits the precise identification of marmoset's pseudoautosomal boundary (PAB) (Fig. 2a). Marmoset PARs harbor nine protein-coding genes, all also found in the human PAR. However, an inversion was found between human and marmoset PARs, and it is likely to occur specifically in the marmoset lineage near its PAB (Fig. 2a and Supplementary Fig. 19). Additionally, downstream of this inversion in the X chromosome, we observed a genomic sequence spanning six human PAR orthologues that had become a new sex-differentiation region (SDR) in the marmoset (Fig. 2a). Three genes in the region, *P2RY8Y*, *AKAP17AY*, and *ZBEDY*, have been reported to be SDR-linked²². We found that they were not collinear with chrX, but were translocated to the middle of chrY (Fig. 2a, Extended Data Fig. 3 and Supplementary Table 26). All the Y copies accumulated more mutations than their corresponding X-copies (Supplementary Fig. 20). Their X-Y genetic divergence was significantly higher than that of the PAR (one-sided t-test, $t = 5.7694$, $p = 1.468 \times 10^{-6}$, Supplementary Table 27), but significantly lower than that of the ancestral SDR (one-sided t-test, $t = -8.9434$, $p = 3.319 \times 10^{-13}$, Supplementary Fig. 21), suggesting that its recombination suppression just recently began. These new SDR genes also showed bias expression in females; however, they were not significantly different from PAR or ancestral SDR genes (Supplementary Fig. 22).

We next applied two divergence-based methods to date the formation of the marmoset specific SDR (MSSDR) (see Supplementary Note, Supplementary Tables 28, 29). Based on the marmoset mutation rate estimated above, we inferred that the MSSDR formed 5.23–9.41 Mya (Supplementary Tables 30, 31). Applying lower mutation rates of the closely related African green monkey (1.11×10^{-9} PPPY)³⁶ and the owl monkey (1.20×10^{-9} PPPY)²³, the MSSDR formation was dated at 6.67–12.97 Mya. All these results indicate that the SDR expansion in the marmoset is an evolutionarily young event.

The translocation of MSSDR on chrY makes the marmoset's PAR the shortest among primates recorded to date²⁴. Since X-Y recombination during male meiosis is limited to the PAR, this region is known to harbor the highest per site recombination rate in the genome²⁵ and increased intensity of GC-biased gene conversion²⁶. Consistently, we observed an elevated GC content in the marmoset PAR relative to human (one-sided t test, $t = 3.1327$, $p = 0.0011$; Supplementary Fig. 21). We also observed a 4.3-fold higher heterozygosity rate of marmoset PAR (0.52%) compared to the average rate in autosomes (0.12%; Supplementary Fig. 23), suggesting that more intense recombination in the shorter marmoset PAR causes more mutations.

Ampliconic genes (AGs), genes with highly similar adjacent copies, is a striking and enigmatic feature of most sex-chromosomes²⁷. They are often found specifically expressed in testis and experience a very rapid turnover of copy number²⁸, leading to the hypothesis that AGs are involved in sexual antagonism²⁸. We detected 22 AGs on the marmoset chrX (Fig. 2b), of which 12 showed testes-restricted expression, at a proportion close to that in humans (40%). Six of the marmoset X-linked AGs were also present in human chrX with overall similar duplication patterns, suggesting they originated from a common ancestor (Fig. 2b and Supplementary Fig. 24). Marmoset chrY also harbors five multi-copy genes of which two (*TSPY* and *RBMY*) are also AGs in human chrY²⁹. These results suggest that the sex-linked AGs have evolved under a very dynamic duplication process during primate evolution.

Rapid evolution of marmoset Y chromosome

In contrast to chrX, which maintained overall conserved synteny during primate evolution (Supplementary Fig. 25), we found that chrY experienced rapid structural changes. This is likely due to the accumulation of mutations as a consequence of Muller's ratchet effect³⁰. We detected at least three large inversions and one large translocation involving genes between the male-specific region of chrY (MSY) of human and marmoset. Human MSY contained 48 protein-coding genes, marmoset MSY contained 46, but with different gene properties (Fig. 3a): 22 human MSY genes were absent in the marmoset; 15 of them evolved during Hominoidea evolution; the rest were ancestral gametologues, but have been inactive or lost in marmoset (Fig. 3a). These included loss of several MSY genes crucial for spermatogenic functions (*HSFY1* and *VCY*; Supplementary Note), or lost function due to frame-shift mutations (*USP9Y*; Supplementary Fig. 26). The loss of these genes in the marmoset might be associated with their monogamous social structures³¹, which potentially alleviates sperm competition. These findings indicate that although it has been claimed that the marmoset has similar spermatogenesis patterns to human³², there are likely some key differences associated with these genes.

In contrast, marmoset MSY only harbors two genes that are absent in human, *ARSHY* and *THOC2Y*. *THOC2Y* was thought to be lost early in the eutherian common ancestor and harbors a high dS value with its gametologue in marsupials³³. However, we found that the marmoset *THOC2Y* has a very low dS value ($dS = 0.0502$) with its X-linked gametologue, suggesting it is not the ancestral but a marmoset specific MSY gene recently duplicated from its X counterpart (Supplementary Fig. 27a). In human, *THOC2* is widely expressed in many tissues and interacts with *XPO4*³⁴ which mediate import of SOX2 and SRY proteins. In the marmoset, both *THOC2X* and *THOC2Y* have become testis-specific genes ($TAU > 0.8$) (Supplementary Fig. 27b). The remaining MSY genes are present in both species, but some with copy number variations (Fig. 3a and Supplementary Fig. 28).

Of the 46 marmoset MSY genes, 18 have their gametologues on chrX (Fig. 3b), and their pairwise dS values between X and Y increased with their distance to the PAB on chrX (Pearson's $r = 0.8342$, $p = 0.0002$; Fig. 3c and Supplementary Table 27) as in humans³⁵. According to the sequence divergence as well as the phylogeny, we inferred the presence of six evolutionary strata in marmoset sex chromosomes, which we named from the oldest to youngest, S1 to S6 (Fig. 3b). S1–S4 are shared with human^{22,35} (Supplementary Fig. 29), suggesting an ancient origin. S5 of the marmoset contained one gametologue pair, *ARSHX-Y*, which has a low pairwise dS (0.0605) close to that of gametologues in MSSDR (Supplementary Table 27). And marmoset's X-copy is clustered with its Y-copy instead of the X-copies of other primates (Supplementary Fig. 30), suggesting this stratum formed specifically in New World Monkeys. S6 contained six pairs of gametologues all residing in MSSDR. Pairwise dS of S6 gametologues are much lower than those of the ancestral gametologues (Fig. 3b). Notably, three gametologues (*DHRX-Y*, *ASMTX-Y*, and *CD99X-Y*) in S6 display the highest pairwise dN/dS values among all gametologues (Supplementary Table 27). Of them, *CD99X* and *CD99Y* show tissue specific expression in ovary and testis, respectively (Supplementary Table 32). These features imply a strong directional selection link to sex differentiation on these genes once they were translocated from the PAR in the marmoset.

Genetic basis of marmoset biological traits

As a representative species of Callitrichidae, the marmoset has many outstanding biological traits, such as small body size³⁶, twinning^{12,37}, exudate-feeding³⁸, and maintaining bone density during aging due to reduced levels of gonadal estrogen, and thus do not suffer from age related osteoporosis^{39,40}. To further expand our knowledge on the evolution of these biological features, we scanned for and identified

204 positively selected genes (PSGs) in the marmoset genome and 38 PSGs in the common ancestor of NWMs (Supplementary Tables 33-35). We have manually checked these PSGs to avoid potential artifacts due to alignment errors or the differences in sequencing and annotation methods across genomes, though we can not fully rule out the possibility that the differences in quality between the compared assemblies may have affected some of these results. Among these genes, we found two that may be linked to manifesting diminutive size. Mutations of *ZDHH13* (PSG in marmoset) in mice causes post-translational lipid modification, resulting in weight loss and reduced bone mineral density⁴¹. *FGFR1* (PSG in NWM) regulates a feedback signal to control the rate of osteoblasts differentiation⁴², and mutations cause autosomal dominant skeletal disorder⁴³. (Supplementary Fig. 31).

Several of the marmosets' unique reproductive adaptations³⁶ include sharing a common placental circulation of siblings⁴⁴ and suppression of reproduction in nondominant females⁴⁵. Previous studies have reported several candidate genes might be related to these traits^{12,37}. We found three marmoset PSGs (*PCSK6*, *NR1D1*, and *TGIF1*) that might also contribute to their reproductive adaptation. *PCSK6* is expressed in numerous ovarian cell types and *PCSK6* mutant mice exhibit progressive loss of ovarian function and formation of ovarian pathology⁴⁶. *NR1D1* is a circadian clock gene and might interact with gonadotropin releasing hormone signaling pathway⁴⁷. Knock out of this gene in mice reduces fertility⁴⁸. *TGIF1* is a repressor and reversibly modulates members of the TGF- β /SMAD signaling pathway, which plays an important role in reproductive processes, including in follicular activation, ovarian follicle development, and oocyte maturation⁴⁹.

We found three marmoset PSGs (*BCL2L14*, *HOMER3*, and *CHADL*) involved in osteoclastogenesis and bone metabolism. *BCL2L14* encodes a member of antiapoptotic proteins, which are known to suppress the functions of osteoclasts⁵⁰. *HOMER3* participates in osteoclastogenesis and bone metabolism. Deletion of this gene significantly decreased tibia bone density, resulting in bone erosion in mice⁵¹. *CHADL* is a collagen-associated small leucine-rich protein and may influence chondrocytes' differentiation by acting on its cellular microenvironment⁵². Further experiments are needed to investigate the potential roles of the positively selected substitutions in specialized bone metabolism in marmosets.

Captive marmosets in labs are intermittently plagued by gastrointestinal disorders⁵³, which may result from dietary differences in captivity versus the wild⁵⁴. Wild marmosets feed on gums as one of their primary food sources, to acquire energy and minerals³⁸. Compared to captive marmosets, the gut microbiome of the wild *Callithrix* is more enriched with *Bifidobacterium*⁵⁵. This probiotic bacterium may function to assist the digestion of gum⁵⁶. We found *PTGS1*, which mediates the gastrointestinal inflammatory reaction, was under positive selection in the marmoset. Expression of this gene is higher in the intestinal mucosa of obese rats^{57,58}, but its expression is reduced to normal levels when fed with *Bifidobacterium*⁵⁸. It seems that *PTGS1* may play a role in marmoset gastrointestinal function, which might be regulated by their exudivore diet through the probiotic bacteria.

Genomic insight on biomedical research

Marmosets are becoming widely used as primate biomedical models in the neurosciences². Here, we compared 2,533 genes related to brain development and neurodegenerative diseases, and found that the majority are highly conserved between marmoset and human in both sequence and copy numbers (Supplementary Fig. 32). However, we detected 24 genes showing copy number variations and 8 genes under diversification selection between the two species. These may be associated with brain differences between human and marmoset (Supplementary Fig. 33, Supplementary Tables 36, 37 and Supplementary Notes).

Pathogenic effects of mutations are highly dependent on their genomic context^{59,60}. We therefore scanned the marmoset genome

for human pathogenic sites that cause or increase risk of nervous system diseases. Interestingly, four genes in marmoset encodes human pathogenic amino acids: *APOE* (C130R), *GBA* (N227S), *SNCA* (A53T), and *PAH* (R176Q) (Supplementary Figs. 34-36 and Supplementary Tables 38). All of them are fixed in the 12 marmoset individuals with genomic data¹³. Comparison with other primates suggests that the *GBA* and *PAH* genomic contexts are unique to the marmoset (Supplementary Figs. 35, 36). The presence of these two pathogenic amino acid types in marmosets suggests this species might have evolved specific mechanisms to compensate for their pathogenic effects, and highlights the critical need to consider genomic context variation when using marmosets as models in human disease research.

Benefits of a diploid assembly

The ultimate goal of creating a reference genome assembly is to produce a gapless, chromosome-level assembly with all sequences fully phased into haplotypes. Several prior efforts have been made towards this goal using the information of a pedigree and/or long reads^{5,6}. Our findings demonstrate the power of using a trio-binning approach, in combination with long-read sequencing^{7,8}, to produce a diploid genome with the two parental haplotypes assembled independently. This method captures the full range of heterozygous variations at high accuracy rates between the two alleles resulting in a heterozygosity rate that is 10 times higher than that found in most genomic studies using only heterozygous SNVs. Our diploid assembly includes more complete sequences for both sex chromosomes, a particular challenge in the case of the Y chromosome with its densely repetitive elements. Whenever trio samples are available, this sequencing and assembly strategy offers the means to generate high-quality, phased reference genomes for a range of species, especially those with high heterozygosity rates.

Online content

Any methods, additional references, Nature Research reporting summaries, source data, extended data, supplementary information, acknowledgements, peer review information; details of author contributions and competing interests; and statements of data and code availability are available at <https://doi.org/10.1038/s41586-021-03535-x>.

- Aleman, F. The necessity of diploid genome sequencing to unravel the genetic component of complex phenotypes. *Front Genet* **8**, 148 (2017).
- Okano, H., Hikishima, K., Iriki, A. & Sasaki, E. The common marmoset as a novel animal model system for biomedical and neuroscience research applications. *Semin Fetal Neonatal Med* **17**, 336-340 (2012).
- Kishi, N., Sato, K., Sasaki, E. & Okano, H. Common marmoset as a new model animal for neuroscience research and genome editing technology. *Dev Growth Differ* **56**, 53-62 (2014).
- Wood, A. R. et al. Allelic heterogeneity and more detailed analyses of known loci explain additional phenotypic variation and reveal complex patterns of association. *Hum Mol Genet* **20**, 4082-4092 (2011).
- Chin, C.-S. et al. Phased diploid genome assembly with single-molecule real-time sequencing. *Nature methods* **13**, 1050-1054 (2016).
- Weisenfeld, N. I., Kumar, V., Shah, P., Church, D. M. & Jaffe, D. B. Direct determination of diploid genome sequences. *Genome Res* **27**, 757-767 (2017).
- Koren, S. et al. De novo assembly of haplotype-resolved genomes with trio binning. *Nat Biotechnol* (2018).
- Rhie, A. et al. Towards complete and error-free genome assemblies of all vertebrate species. *bioRxiv*, 2020.2005.2022.110833 (2020).
- Sherlock, J. K., Griffin, D. K., Delhanty, J. D. A. & Parrington, J. M. Homologies between human and marmoset (*Callithrix jacchus*) chromosomes revealed by comparative chromosome painting. *Genomics* **33**, 214-219 (1996).
- Benirschke, K., Anderson, J. M. & Brownhill, L. E. Marrow chimerism in marmosets. *Science* **138**, 513-515 (1962).
- Sweeney, C., Ward, J. & Vallender, E. J. Naturally occurring, physiologically normal, primate chimeras. *Chimerism* **3**, 43-44 (2012).
- Marmoset Genome, S. & Analysis, C. The common marmoset genome provides insight into primate biology and evolution. *Nat Genet* **46**, 850-857 (2014).
- Sato, K. et al. Resequencing of the common marmoset genome improves genome assemblies and gene-coding sequence analysis. *Sci Rep* **5**, 16894 (2015).
- Nembaware, V., Wolfe, K. H., Bettoni, F., Kelso, J. & Seoghe, C. Allele-specific transcript isoforms in human. *FEBS Lett* **577**, 233-238, <https://doi.org/10.1016/j.febslet.2004.10.018> (2004).

15. Anton, E., Blanco, J. & Vidal, F. Meiotic behavior of three D; G Robertsonian translocations: segregation and interchromosomal effect. *Journal of human genetics* **55**, 541-545 (2010).
16. Stankiewicz, P. & Lupski, J. R. Genome architecture, rearrangements and genomic disorders. *Trends in Genetics* **18**, 74-82 (2002).
17. Acuna-Hidalgo, R., Veltman, J. A. & Hoischen, A. New insights into the generation and role of de novo mutations in health and disease. *Genome Biol* **17**, 1-19 (2016).
18. Goldmann, J. M. et al. Parent-of-origin-specific signatures of de novo mutations. *Nat Genet* **48**, 935-939 (2016).
19. Chintalapati, M. & Moorjani, P. Evolution of the mutation rate across primates. *Current Opinion in Genetics & Development* **62**, 58-64 (2020).
20. Zoonomia, C. A comparative genomics multitool for scientific discovery and conservation. *Nature* **587**, 240 (2020).
21. Vollger, M. R. et al. Long-read sequence and assembly of segmental duplications. *Nat Methods* **16**, 88-94 (2019).
22. Bellott, D. W. et al. Mammalian Y chromosomes retain widely expressed dosage-sensitive regulators. *Nature* **508**, 494-499 (2014).
23. Thomas, G. W. C. et al. Reproductive Longevity Predicts Mutation Rates in Primates. *Curr Biol* **28**, 3193-3197 e3195 (2018).
24. Raudsepp, T. & Chowdhary, B. P. The Eutherian Pseudoautosomal Region. *Cytogenet Genome Res* **147**, 81-94 (2015).
25. Hinch, A. G., Altemose, N., Noor, N., Donnelly, P. & Myers, S. R. Recombination in the human pseudoautosomal region PAR1. *PLoS Genet* **10**, e1004503 (2014).
26. Holmquist, G. P. Chromosome bands, their chromatin flavors, and their functional features. *Am J Hum Genet* **51**, 17-37 (1992).
27. Hughes, J. F. & Page, D. C. The biology and evolution of mammalian Y chromosomes. *Annu Rev Genet* **49**, 507-527 (2015).
28. Mueller, J. L. et al. Independent specialization of the human and mouse X chromosomes for the male germ line. *Nat Genet* **45**, 1083-1087 (2013).
29. Lucotte, E. A. et al. Dynamic copy number evolution of X- and Y-linked ampliconic genes in human populations. *Genetics* **209**, 907-920 (2018).
30. Bachtrog, D. A dynamic view of sex chromosome evolution. *Curr Opin Genet Dev* **16**, 578-585 (2006).
31. Wahab, F., Drummer, C. & Behr, R. Marmosets. *Curr Biol* **25**, R780-782 (2015).
32. Millar, M. R., Sharpe, R. M., Weinbauer, G. F., Fraser, H. M. & Saunders, P. T. Marmoset spermatogenesis: organizational similarities to the human. *Int J Androl* **23**, 266-277 (2000).
33. Cortez, D. et al. Origins and functional evolution of Y chromosomes across mammals. *Nature* **508**, 488-493 (2014).
34. Havugimana, P. C. et al. A census of human soluble protein complexes. *Cell* **150**, 1068-1081 (2012).
35. Lahn, B. T. & Page, D. C. Four evolutionary strata on the human X chromosome. *Science* **286**, 964-967 (1999).
36. Abbott, D. H., Barnett, D. K., Colman, R. J., Yamamoto, M. E. & Schultz-Darken, N. J. Aspects of common marmoset basic biology and life history important for biomedical research. *Comp Med* **53**, 339-350 (2003).
37. Harris, R. A. et al. Evolutionary genetics and implications of small size and twinning in callitrichine primates. *Proc Natl Acad Sci U S A* **111**, 1467-1472 (2014).
38. Power, M. L. in *The evolution of exudativory in primates* 25-44 (Springer, 2010).
39. Colman, R. J. Absence of estrogen depletion bone loss in female common marmosets. *J Bone Miner Res* **12**, S342 (1997).
40. Binkley, N. et al. Zoledronate prevents the development of absolute osteopenia following ovariectomy in adult rhesus monkeys. *J Bone Miner Res* **13**, 1775-1782 (1998).
41. Saleem, A. N. et al. Mice with alopecia, osteoporosis, and systemic amyloidosis due to mutation in *Zdhhc13*, a gene coding for palmitoyl acyltransferase. *PLoS Genet* **6**, e1000985 (2010).
42. Iseki, S., Wilkie, A. O. & Morriss-Kay, G. M. *Fgfr1* and *Fgfr2* have distinct differentiation-and proliferation-related roles in the developing mouse skull vault. *Development* **126**, 5611-5620 (1999).
43. White, K. E. et al. Mutations that cause osteoglyphonic dysplasia define novel roles for *FGFR1* in bone elongation. *The American Journal of Human Genetics* **76**, 361-367 (2005).
44. Moore, H. D. M., Gems, S. & Hearn, J. P. Early implantation stages in the marmoset monkey (*Callithrix jacchus*). *American Journal of Anatomy* **172**, 265-278 (1985).
45. Saltzman, W., Schultz-Darken, N. J., Severin, J. M. & Abbott, D. H. Escape from social suppression of sexual behavior and of ovulation in female common marmosets. *Ann N Y Acad Sci* **807**, 567-570 (1997).
46. Mujoomdar, M. L., Hogan, L. M., Parlow, A. F. & Nachtigal, M. W. *Pcsk6* mutant mice exhibit progressive loss of ovarian function, altered gene expression, and formation of ovarian pathology. *Reproduction* **141**, 343-355 (2011).
47. Cho, H. et al. Regulation of circadian behaviour and metabolism by *REV-ERB-α* and *REV-ERB-β*. *Nature* **485**, 123-127 (2012).
48. Chomez, P. et al. Increased cell death and delayed development in the cerebellum of mice lacking the *rev-erbA(α)* orphan receptor. *Development* **127**, 1489-1498 (2000).
49. Zhang, Z. et al. *TGIF1* and *SF1* polymorphisms are associated with litter size in Small Tail Han sheep. *Reprod Domest Anim* **55**, 1145-1153 (2020).
50. Lagasse, E. & Weissman, I. L. Enforced expression of *Bcl-2* in monocytes rescues macrophages and partially reverses osteopetrosis in *op/op* mice. *Cell* **89**, 1021-1031 (1997).
51. Son, A. et al. *Homer2* and *Homer3* modulate *RANKL*-induced *NFATc1* signaling in osteoclastogenesis and bone metabolism. *J Endocrinol* **242**, 241-249 (2019).
52. Tillgren, V., Ho, J. C. S., Önnérjod, P. & Kalamajski, S. The novel small leucine-rich protein chondroadherin-like (*CHADL*) is expressed in cartilage and modulates chondrocyte differentiation. *Journal of Biological Chemistry* **290**, 918-925 (2015).
53. Ludlage, E. & Mansfield, K. Clinical care and diseases of the common marmoset (*Callithrix jacchus*). *Comp Med* **53**, 369-382 (2003).
54. Bailey, M. T. & Coe, C. L. Intestinal microbial patterns of the common marmoset and rhesus macaque. *Comparative Biochemistry and Physiology Part A: Molecular & Integrative Physiology* **133**, 379-388 (2002).
55. Malukiewicz, J. et al. The gut microbiome of exudivorous wild and captive marmosets. *bioRxiv*, 708255 (2020).
56. Turroni, F. et al. Glycan utilization and cross-feeding activities by *Bifidobacteria*. *Trends Microbiol* **26**, 339-350 (2018).
57. Wisniewski, J. R., Friedrich, A., Keller, T., Mann, M. & Koepsell, H. The impact of high-fat diet on metabolism and immune defense in small intestine mucosa. *J Proteome Res* **14**, 353-365 (2015).
58. Plaza-Diaz, J. et al. *Adamdec1*, *Ednrb* and *Ptgs1/Cox1*, inflammation genes upregulated in the intestinal mucosa of obese rats, are downregulated by three probiotic strains. *Sci Rep* **7**, 1939 (2017).
59. Jordan, D. M. et al. Identification of cis-suppression of human disease mutations by comparative genomics. *Nature* **524**, 225-229 (2015).
60. Storz, J. F. Compensatory mutations and epistasis for protein function. *Curr Opin Struct Biol* **50**, 18-25 (2018).

Publisher's note Springer Nature remains neutral with regard to jurisdictional claims in published maps and institutional affiliations.



Open Access This article is licensed under a Creative Commons Attribution 4.0 International License, which permits use, sharing, adaptation, distribution and reproduction in any medium or format, as long as you give appropriate credit to the original author(s) and the source, provide a link to the Creative Commons license, and indicate if changes were made. The images or other third party material in this article are included in the article's Creative Commons license, unless indicated otherwise in a credit line to the material. If material is not included in the article's Creative Commons license and your intended use is not permitted by statutory regulation or exceeds the permitted use, you will need to obtain permission directly from the copyright holder. To view a copy of this license, visit <http://creativecommons.org/licenses/by/4.0/>.

© The Author(s) 2021

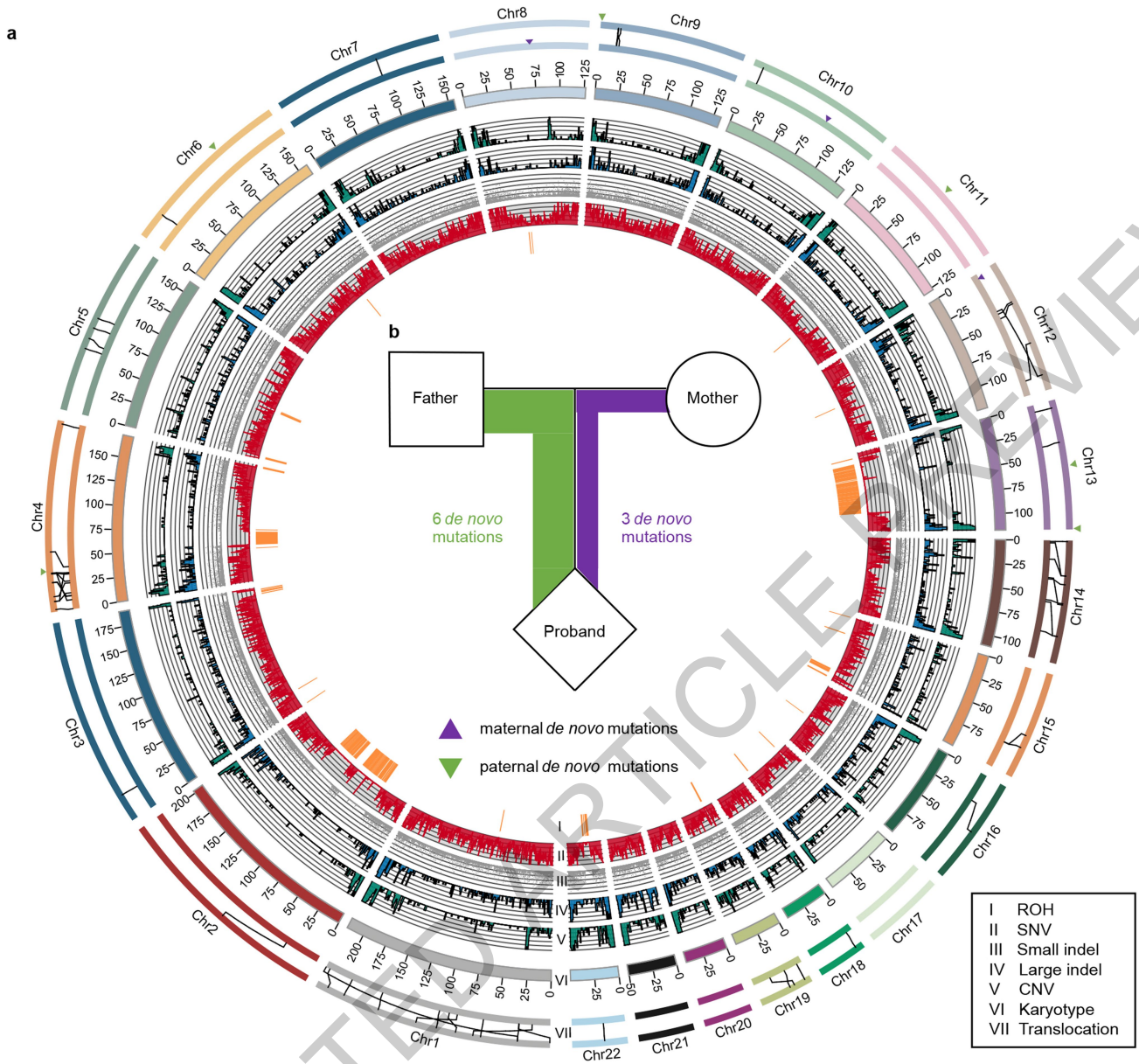


Fig. 1 | The distribution of SNVs, small indels, and SVs in a diploid marmoset genome. a, Heterozygosity landscape patterns between the two haploid marmoset genomes. Tracks from inside out: distribution of ROH (>1 Mb), SNV density (window size 500kb, range 0-0.85%), small indel (<50 bp) distribution (y-axis: indel length), large indel density (≥50 bp, window size 1 Mb, count 0-9),

CVN density (window size 1 Mb, count 0-9). The links in the outermost circles denote translocation event differences between maternal (inner) and paternal (outer) assemblies (VII). Triangles, locations of the *de novo* mutations in parental alleles. **b**, Schematic diagram showing the proportion of parental sources of the *de novo* mutations.

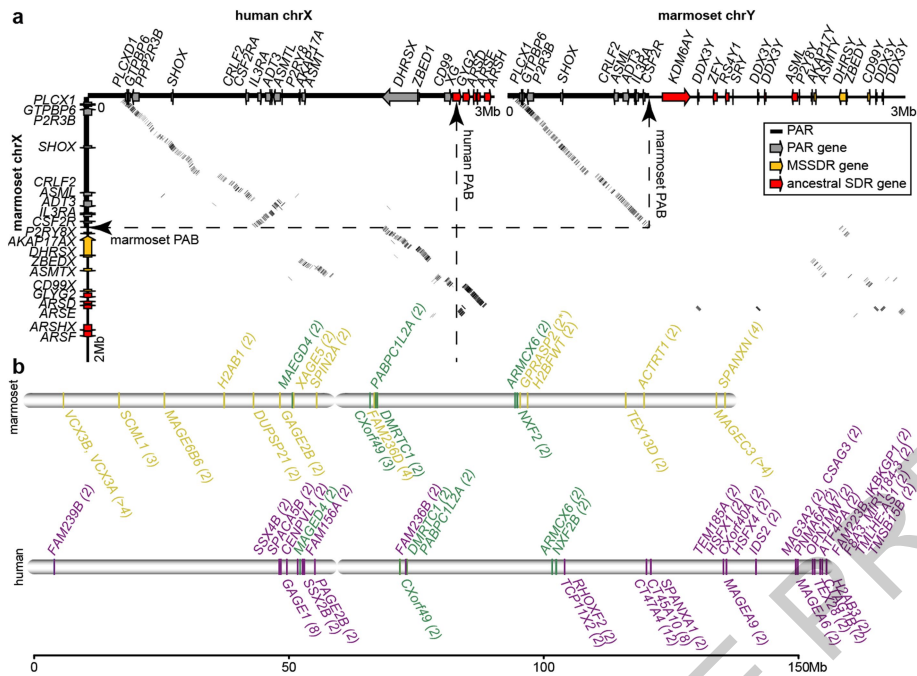


Fig. 2 | Marmoset versus human sex chromosome structures. a, Alignment between the marmoset X and Y reveals a ~1 Mb PAR in each chromosome. Dashed lines show the boundaries between the PAR and SDR. Alignment between the human and marmoset X also reveals different PABs between the two species, and an inversion near the marmoset PAB. Grey, PAR gene; orange,

MSSDR genes; red, ancestral SDR genes. **b**, Distribution of AGs in the marmoset (yellow) and human (purple) chrX. Green, genes that are ampliconic in both species. Copy number for each AG is shown in brackets. AGs with testis-specific expressions are shown at the bottom panel.

Methods

Sample collection, processing, and sequencing

Samples were collected at an AAALAC accredited facility from an F1 male marmoset (3 months) at The Rockefeller University, USA, under USDA and IACUC approved protocols. Quadriceps muscle was dissected, harvested, and flash frozen in liquid nitrogen immediately following euthasol administration; we extracted genomic DNA from the muscle sample. This DNA was used for Bionano optical mapping, PacBio library preparation and SMRT sequencing, 10x Genomics linked-read sequencing, and Arima Hi-C / Illumina sequencing. We collected blood samples from both of the F1 male's parents (mother: 3 years 10 months, father: 3 years 7 months) for Illumina sequencing by shaving the area (thigh for saphenous vein and tail for lateral tail vein), applying 2% lidocaine jelly, prepping the vein with alcohol, and collecting <2 mls blood per sample (1x sample for male and female) via IV blood draw into EDTA tubes.

For annotation purposes, we collected 18+ tissues from the F1 male's brother. Blood was collected from the saphenous vein pre-mortem using the method described above. All additional tissues were dissected, harvested, and flash frozen in liquid nitrogen or powdered dry ice immediately following euthasol administration; brain and testes were dissected at first and all tissues were dissected and frozen with a 30 min period post-mortem. RNA integrity numbers (RINs) for all tissues used for PacBio SMRT sequencing and Iso-Seq analysis ("Sample processing and sequencing" section in Supplementary Note) were high, ranging from 8.2 (lung) to 9.9 (cerebellum). We performed mashmap quality control analyses of sequencing reads to rule out any potential contamination or poor sequencing prior to assembling (Supplementary Fig. 1).

Statement about sample size choice, randomization, and blinding

We aim to use parental SNVs to determine and phase the offspring's two haplotype genomes, thus the sample size for genome sequencing is three. Bioinformatic analyses were performed with all available data. Randomization for genome and transcriptome sequencing is not applied in this study. For SNV and indel PCR validation, variation sites were randomly selected by Linux command "sort -R". Blinding was not necessary for genome and transcriptome sequencing or genetic variation PCR validation. The study aims to identify the genetic differences inherited from parental genomes, so only the F1 individual's DNA sample was used for PCR validation.

Genome assembly

We combined the trio-binning approach initially developed by Koren et al.⁷ and further advanced the Vertebrate Genomes Project (VGP) assembly pipeline by Rhie et al.⁸ for scaffolding, to generate the haplotype-phased marmoset assembly (Supplementary Fig. 2). In the first step, we used TrioCanu (v1.8+287) to bin PacBio long reads of the F1 male into maternal and paternal haplotypes using haplotype-specific 21-mer markers generated from the Illumina short reads of the mother and father. Following binning, TrioCanu independently generated contigs for each haplotype (haplotigs). From here on, the maternal and paternal haplotigs underwent the same steps independently. Separately, we assembled the mitochondrial (MT) genome with the mitoVGP pipeline (v2.2)⁶¹ and added it to the haplotigs to keep any raw MT reads from being mapped to nuclear sequences, which would result in lower sequence quality after polishing. We used Arrow from smrtlink (v6.0.0.47841) to improve base calling accuracy and purge_dups (v1.0.0)⁶² in an adapted trio mode to remove overlaps at the ends of contigs. The resulting polished, purged haplotigs were scaffolded in three stages: first, we used the 10x linked-reads in two rounds of scaff10x (v4.1.0) (<https://github.com/wtsi-hpag/Scaff10X>) to generate the primary scaffolds; second, we generated Bionano cmaps and

used Bionano Solve (v3.2.1_04122018)⁶³ for hybrid scaffolding and to break mis-assemblies; third, we used Salsa2 (v2.2)⁶⁴ to generate chromosomal-level scaffolds using the molecular contact information from Hi-C linked reads. Finally, we performed a second round of Arrow polishing on the maternal and paternal scaffolds with the binned long reads. During this round of polishing, gaps between contigs were closed by the gap-filling function of Arrow. The parental haplotypes were then combined in a single assembly and underwent two rounds of short read polishing using longranger (v2.2.2)⁶⁵ for short read alignment and freebayes (v1.3.1)⁶⁶ for polishing (Supplementary Note). After splitting the scaffolds by haplotype and removing the MT genome from each assembly, the two assemblies (named mCalJac1.mat and mCalJac1.pat) underwent manual curation using the gEVAL tool⁶⁷, particularly to correct structural assembly errors. In the abbreviated name, m = mammal; CalJac is the abbreviated latin species name; 1 is the first VGP assembly of this species; mat and pat are maternal and paternal haplotypes, respectively.

Sex-linked sequence identification and additional Y chromosome assembly

To identify X-linked and Y-linked sequences in mCalJac1 (GCA_011100555.1) we mapped parental short reads to the assembly with BWA ALN (v0.7.12)⁶⁸. Coverage was extracted with SAMTools (v1.2) and normalized by the peak coverage. In X-linked sequences identification, normalized female-vs-male (F/M) coverage ratio was calculated and plotted in a 5-kb window size, and scaffolds with F/M coverage ratio within range 1.5 to 2.5 were identified as X-linked. In Y-linked sequence identification, normalized F/M coverage ratio was calculated and plotted in a 2-kb window size and scaffolds with F/M coverage ratio within a 0.0 to 0.3 range were identified as Y-linked. We further manually examined large scaffolds in the maternal and paternal assemblies and included the Y chromosome Super_scaffold_pat_24. This scaffold was missing in the 0.3 cutoff condition because the first 1 Mb sequence shows an equal female and male coverage PAR pattern.

In these previous steps, only ~6 Mb Y-linked sequences were identified, about 14 Mb smaller than the expected 20 Mb size based on karyotyping. Since sex chromosomes are notoriously difficult to assemble, and no primate has had a complete Y chromosome sequenced, to determine if we missed any Y chromosomal sequences, we performed additional assembly steps. We utilized Hi-C interaction information to call back potential Y-linked contigs that were filtered by our strict filtering based on half sex-chromosome read depths. Arima Hi-C reads were mapped to mCalJac1 and the Hi-C interaction matrix was generated by HiCPro (v2.10.0)⁶⁹. Under 10kb resolution, we extracted the interaction strength of every unplaced scaffold to each autosome, X or Y chromosomes. Unplaced scaffolds with more than five interaction strength values to both autosomes/X and Super_scaffold_pat_24 were selected, and the interaction strength with the autosomes/X and the interaction strength with Y was compared for each scaffold by two-sided Wilcoxon rank-sum test. With a false discovery rate (FDR) corrected *p* value cutoff of 0.01, we further identified 17 scaffolds that show significantly higher interaction with Super_scaffold_pat_24 than with other chromosomes, and considered them putative Y-linked scaffolds. To validate this result, we collected marmoset Y-BAC sequences from NCBI and mapped them to mCalJac1 with minimap2. Almost all BAC sequences mapped to the eight Y-linked scaffolds were identified by the sequencing depth method. One, BAC AC279170.1, was previously missed, but can now be mapped to pat_scaffold_39_arrow_ctg1, which was identified by the Hi-C method. Thus, the dataset identified by the Hi-C method complements the dataset identified by the sequencing depth method. Combining these two datasets, a total of 25 potential Y-linked scaffolds (~14.13Mb) were identified from mCalJac1 (Supplementary Table 39).

Next, we mapped the PacBio raw reads to the assembly and found that some of the potentially Y-linked scaffolds had regions of considerably

Article

high coverage compared to autosomes and X chromosomes, indicative of collapsed sequences, which would cause the artificially high level Hi-C interaction and introduce false-positive Y-linked sequences. To de-collapsed these regions, we used the Segmental Duplication Assembler (SDA)²¹ and mapped the SDA assembled contigs to their original scaffolds with minimap2 to remove potential assembly artifacts. In order to replace the original collapsed sequence in the assembly with the most plausible candidate decollapsed sequence, we applied “the longest rule”: start with the de-collapsed sequence in the SDA output that has the longest stretch mapping back to the original scaffold, then select the second sequence with the longest match that doesn’t overlap the previous one, etc. Once all the non-overlapping decollapsed sequences with the longest matches were selected, we filled in the gaps using the original scaffold as backbone, and left 1,000 Ns between each contig.

To further exclude false positives from the de-collapsed Y dataset, we refiltered the sequences with the sex-differential depth ratio and the Hi-C interaction criteria as mentioned above (Supplementary Table 24). However, since only the uniquely mapped reads were used in calculating the Hi-C interaction between unplaced scaffolds and autosomes/X/Y, our results underestimate Y chromosomal DNA, including many de-collapsed Y scaffolds with multiple copies that might still be missed.

SNP, indel, and SV detection using whole haplotype genome alignment

To call heterozygous sites between the two haploid sequences, independent of the GenomeScope calculation, we first performed a Mummer (v3.23) alignment with the parameters of “nucmer -maxmatch -l 100 -c 500”. Because our assemblies span most repetitive sequences, repeat-masking treatment was not necessary before conducting the Mummer alignment. A series of custom scripts (<https://github.com/comery/marmoset>) identified and sorted our SNPs, indels in the alignments. We employed svmu (v0.4-alpha)⁷⁰, Assemblytics (v1.2)⁷¹, and SyRi (v1.0)⁷², to detect SVs from Mummer alignment. After several test rounds, we found that svmu reported more accurate large indels, and Assemblytics detected CNVs, particularly tandem repeats, whereas SyRi detected other SVs well. We employed these three methods and combined the results as confident SVs. We used default parameters for svmu, Assemblytics, and recommended nucmer alignment for SyRi (<https://schneebergerlab.github.io/syri/>)

To generate a high-quality SV dataset, we manually checked all inversions and translocations with the following steps: a) clip 300 bp of upstream/downstream flanking sequence of each breakpoint between the two haplotypes, blast against local PacBio reads with threshold identity >96% and aligned length >550 bp, and require the SV region where the maternal and paternal sequences aligned to have high similarity (>90%); b) if (a) failed, then check the 10X linked-read count between a 5 kb flanking region; c) if any breakpoint is not supported by 10X linked-reads, check the Hi-C heatmap of this region; if it shows an inversion or translocation pattern on heatmap or an ambiguous situation, then remove it.

To evaluate the accuracy of SV detection, we searched the binned PacBio reads around the breakpoints of both maternal and paternal assemblies for all indels in chromosome 1. We looked for one of the following three features to determine the indel as accurate: i) at least one single PacBio long read from each haplotype that spans the entire indel region with the variation found in each haplotype; ii) have overlapping PacBio reads that span the two breakpoints; or iii) manually validated PacBio read alignment by Integrative Genomics Viewer (IGV)⁷³. Finally, we found 95.7% of indels are correct when considering the breakage location; however, 74.2% are accurate when considering both boundary and location.

Sequencing error and polishing error estimation

To calculate sequencing errors and polishing errors, we established a confident SNP set as a criterion. We used three individual approaches

to detect SNPs between two haplotypes: 1) retrieved heterozygous sites from the Mummer alignment between the maternal and paternal haplotypes excluding the sex chromosomes (setA, containing 3.48 MSNVs); 2) GATK pipeline based on mapping of 10X linked-reads from the F1 offspring (setB); and 3) samtools (v1.8) mpileup followed by bcftools also based on 10X linked-reads mapping (setC). Then, a raw SNP dataset was generated by a two-step procedure: first taking the intersection of setB and setC to generate Set1 (3.72 M SNVs), followed by taking the union of setA and Set1 to get Set2 (3.77 M SNVs). We then took these two sets and selected among them to a high-quality 3.58 MSNVs Set3 (Supplementary Fig. 10) with the following criteria applied: 1) 10X linked-read depth lower than 10; 2) filter out sites which do not align to the two haplotype assemblies; 3) filter out sites which we could not call a typical haplotype based on much less than 50% nucleotide distribution ($\pi > 0.4$ & the third highest depth > 5, where π is calculated as: $\pi = 2 * (A * T + A * C + A * G + T * C + T * G + C * G) / (totalDepth * (totalDepth - 1))$ and A, T, C, G represent the sequencing depth of base A, T, C, G for each site. For example, a distribution of “A:20; T:20; C:14; G:0” indicates a complex condition. We also collected the mapping information from raw PacBio reads and corrected PacBio reads. This allowed us to establish an evidence chain of how the bases in each haplotype changed during assembling and polishing, which allowed us to classify different error types. We classified 195,751 sequencing error sites and 180,712 polishing error sites. The sequencing and polishing error rates were estimated to be 3.41×10^{-5} and 3.66×10^{-5} , respectively. We further validated the variants with PCR experiments. (see Supplementary Note).

Mutation rate analysis

The F1 offspring’s 10X linked-reads and the parents’ short reads were mapped to each genome assembly independently (paternal and maternal assemblies). Duplicate reads and reads mapping to more than one region were removed. Variants were called using GATK4 HaplotypeCaller in base-pair resolution mode, calling each single site of the genome. Two independent joint genotypes were produced: one for the 3 individuals (mother, father, and F1 offspring) mapped to the maternal assembly and one for the 3 individuals mapped to the paternal assembly. We identified a maternal candidate *de novo* mutation as a site where the parents were homozygous for the reference (0/0) and the offspring was heterozygous (0/1) when mapped to the paternal genome. For validation, such a candidate site would be expected to have the parents homozygous for the alternative (1/1), and the offspring heterozygous (0/1) when mapped to the maternal genome. Similarly, a paternal candidate *de novo* mutation was identified as such in a site where the parents were homozygous for the reference (0/0), and the offspring was heterozygous (0/1) when mapped to the maternal genome. Here, again, those candidates were validated if they also appeared in the parents as homozygous for the alternative (1/1), and in the offspring heterozygous (0/1) when mapped to the paternal genome. Additional filters were applied for sites, genotype quality, read depth, and number of alternative alleles in the parents and allelic balance in the offspring (Supplementary Note). Finally, we removed any potential sites with sequencing errors, polishing errors, or assigning errors, as well as sites that failed the PCR validation. To calculate a rate, we computed the number of callable sites in each genome as the number of sites where both parents were homozygous for the reference and all individuals passed the depth coverage between half and two times the average depth for each individual, number of alternative alleles allowed, and genotype quality filters. We corrected those callable sites by a negative rate factor, alpha (α), which is the percentage of callable sites that would be filtered away by our site filters (following known distribution) and the allelic balance filter (which corresponds to the number of sites where one parent was homozygous for the reference allele, the other parent was homozygous for the alternative allele, and the offspring would be heterozygous, but

the reads supporting each allele would be outside our allelic balance filter). The mutation rate was calculated as:

$$\mu = \frac{nb \text{ mutation}_{maternal} + nb \text{ mutations}_{paternal}}{Callability_{maternal} \times (1 - \alpha_{maternal}) + Callability_{paternal} \times (1 - \alpha_{paternal})}$$

Y-linked sequences order confirmation

Marmoset Y-specific BAC end reads²² were obtained from NCBI trace archive and mapped to Y-linked sequences with BWA MEM. Only the primary alignment was kept for each read. BAC location on Y from²² was also obtained and visualized in a dotplot to confirm the order of the Y-linked sequences in mCalJac1. To confirm the MSSDR translocation in Y, we further checked PacBio and 10X linked reads support at the flanking breakpoint of the Y MSSDR.

Detection of positive selection genes

We used BLAST Reciprocal Best Hits (RBH) method (Supplementary Note) to identify high-confidence one-to-one orthologous genes among species, including three other NWMs (white-faced capuchin (*Cebus capucinus*), Ma's night monkey (*Aotus nancymae*), and black-capped squirrel monkey (*Saimiri boliviensis*)); three old world primates (human (*Homo sapiens*), macaque (*Macaca mulatta*), and chimpanzee (*Pan troglodytes*)); and three outgroups (treeshrew (*Tupaia glis*), mice (*Mus musculus*), and cow (*Bos taurus*)). The marmoset was set as foreground when detecting marmoset-specific PSGs, while the NWM were set as foreground when detecting NWM-specific PSGs. A total of 13,995 one-to-one orthologous genes were identified. To minimize the effect of gene annotation, we retrieved the corresponding CDS that shared the same isoform with human. These genes were used as an input dataset to conduct multiple sequence alignment using PRANK (v170427)⁷⁴ and guidance (v2.02)⁷⁵ to improve the alignment. The positive selection sites within a specific lineage were detected by branch-site model in PAML (v4.9i)⁷⁶. Genes with an FDR-adjusted p value less than 0.05 were treated as candidates for positive selection. To minimize effects of assembly and alignment, we filtered candidate PSGs if 1) the positive selective site was gap in more than two species; 2) the PS sites have more than two nonsynonymous substitution forms (ignoring outgroup), and 3) the flanking region (± 10 amino acids) have over-alignment across species. We also performed a manual check for all individual PSGs to avoid any other false-positive caused by annotation or alignment. Finally, we used read mapping to check the PSG sites to avoid sequencing errors. After filtering, the numbers of PSGs with high confidence detected in marmoset and NWM were 204 and 38, respectively.

Scan for pathogenic or risky mutations in marmoset

Mutation information was obtained from ClinVar (https://ftp.ncbi.nlm.nih.gov/pub/clinvar/tab_delimited/variant_summary.txt.gz, on 30/06/2020) and mutations that were designated to be pathogenic or risky were extracted. Nervous system related mutations were extracted with keywords "Adrenoleukodystrophy, Alzheimer, Amyotrophic lateral sclerosis, Angelman, Ataxia telangiectasia, Charcot-Marie-Tooth, Cockayne, Deafness, Duchenne muscular dystrophy, Epilepsy, Fragile X syndrome, Friedreich ataxia, Gaucher, Huntington, Lesch-Nyhan syndrome, Maple syrup urine disease, Menkes syndrome, Myotonic dystrophy, Narcolepsy, Neurofibromatosis, Niemann-Pick disease, Parkinson disease, Phenylketonuria, Refsum disease, Rett syndrome, Spinal muscular, Spinocerebellar ataxia, Tangier disease, Tay-Sachs disease, Tuberous sclerosis, Von Hippel-Lindau syndrome, Wilson disease". Related protein sequences of human and marmoset were extracted and aligned with PRANK and targeted amino acid sites were scanned to determine if the human pathogenic/risky mutation is in the marmoset. The genomic coordinates of related codons were extracted to check the alignment of the 12 marmoset individuals with whole genome

sequencing data. Alignment was visualized and manually examined with Jalview (v2.11.1.0)⁷⁷.

Reporting summary

Further information on research design is available in the Nature Research Reporting Summary linked to this paper.

Data availability

Raw sequencing data for the marmoset trio is available under the GenomeArk github (https://vgp.github.io/genomeark/Callithrix_jacchus/). Curatorial information and data mappings to maternal and paternal assemblies are available on the genome evaluation browser, gEVAL (https://vgp-geval.sanger.ac.uk/all_genomes.html). The maternal, paternal, and combined (paternal autosomes and Y chromosome + maternal X chromosome + mitochondrial) assemblies, as well as PacBio Iso-Seq data for annotation, are available under the NCBI BioProject PRJNA560230 (<http://www.ncbi.nlm.nih.gov/bioproject/PRJNA560230>). The genome assemblies have also been deposited at CNSA of CNGBdb with accession CNP0001310 and CNP0001311.

Code availability

The assembly pipeline is on Github (<https://github.com/VGP/vgp-assembly>); see Supplementary Tables 2, 3 for the full list of tools used, versions, and availability. Workflows and applets built for the VGP are available on DNAnexus (<https://www.dnanexus.com/>). Custom scripts are available at <https://github.com/comery/marmoset> and <https://github.com/gf777/misc/tree/master/marmoset%20Y>.

- Formenti, G. et al. Complete vertebrate mitogenomes reveal widespread gene duplications and repeats. *bioRxiv*, 2020.2006.2030.177956 (2020).
- Guan, D. et al. Identifying and removing haplotypic duplication in primary genome assemblies. *Bioinformatics* **36**, 2896-2898 (2020).
- Lam, E. T. et al. Genome mapping on nanochannel arrays for structural variation analysis and sequence assembly. *Nat Biotechnol* **30**, 771-776 (2012).
- Ghurye, J. et al. Integrating Hi-C links with assembly graphs for chromosome-scale assembly. *PLoS Comput Biol* **15**, e1007273 (2019).
- Bishara, A. et al. Read clouds uncover variation in complex regions of the human genome. *Genome Res* **25**, 1570-1580 (2015).
- Garrison, E. & Marth, G. Haplotype-based variant detection from short-read sequencing. *arXiv preprint arXiv:1207.3907* (2012).
- Chow, W. et al. gEVAL - a web-based browser for evaluating genome assemblies. *Bioinformatics* **32**, 2508-2510 (2016).
- Li, H. & Durbin, R. Fast and accurate short read alignment with Burrows-Wheeler transform. *Bioinformatics* **25**, 1754-1760 (2009).
- Servant, N. et al. HiC-Pro: an optimized and flexible pipeline for Hi-C data processing. *Genome Biol* **16**, 259 (2015).
- Chakraborty, M., Emerson, J. J., Macdonald, S. J. & Long, A. D. Structural variants exhibit widespread allelic heterogeneity and shape variation in complex traits. *Nat Commun* **10**, 4872 (2019).
- Nattestad, M. & Schatz, M. C. Assemblytics: a web analytics tool for the detection of variants from an assembly. *Bioinformatics* **32**, 3021-3023 (2016).
- Goel, M., Sun, H., Jiao, W. B. & Schneeberger, K. SyRI: finding genomic rearrangements and local sequence differences from whole-genome assemblies. *Genome Biol* **20**, 277 (2019).
- Robinson, J. T. et al. Integrative genomics viewer. *Nat Biotechnol* **29**, 24-26 (2011).
- Loytynoja, A. Phylogeny-aware alignment with PRANK. *Methods Mol Biol* **1079**, 155-170 (2014).
- Sela, I., Ashkenazy, H., Katoh, K. & Pupko, T. GUIDANCE2: accurate detection of unreliable alignment regions accounting for the uncertainty of multiple parameters. *Nucleic Acids Res* **43**, W7-14 (2015).
- Yang, Z. PAML 4: phylogenetic analysis by maximum likelihood. *Mol Biol Evol* **24**, 1586-1591 (2007).
- Waterhouse, A. M., Procter, J. B., Martin, D. M., Clamp, M. & Barton, G. J. Jalview Version 2—a multiple sequence alignment editor and analysis workbench. *Bioinformatics* **25**, 1189-1191 (2009).

Acknowledgements This work was supported by Strategic Priority Research Program of the Chinese Academy of Sciences (XDB31020000), the National Key R&D Program of China (MOST) grant 2018YFC1406901, International Partnership Program of Chinese Academy of Sciences (No. 152453KY5B20170002), Carlsberg foundation (CF16-0663), Villum Foundation (No. 25900) to G.Z. Howard Hughes Medical Institute and Rockefeller University start up funds to E.D.J. Intramural Research Program of the National Human Genome Research Institute, National Institutes of Health (A.R., A.M.P., and S.K.), Korea Health Technology R&D Project through the Korea Health Industry Development Institute H17C2098 (A.R.), and the NIH

Article

National Institute of General Medical Sciences (No. T32GM007739) and an NIH National Institute of Mental Health F30 (No. MH112351) (M.M.F.), and Guangdong Provincial Academician Workstation of BGI Synthetic Genomics (No. 2017B090904014) (H.Y).

Author contributions G.Z. and E.D.J. initiated and designed the project. S.M., J.M., B.H., J.Ba., M.M.F., O.F., W.A.F., and H.Y. coordinated and performed sample collection and sequencing. S.M., G.F., J.W., W.C., K.H., A.R., M.P., A.M.P., S.K., Y.Zhou, X.B., Z.S., and G.Z. performed genome assembling, curation, and evaluation. C.Y., Y.Zhou, S.M., and G.F. performed the chimeric analysis. C.Y., L.B., X.B., C.Z., and G.Z. performed genetic diversity analysis. L.B. and G.Z. calculated mutation rate. C.Y. and S.T. performed experiment validation. Y.Zhou, L.Z., J.Be., M.M.R., G.Z., and M.H.S. performed analysis of sex chromosomes. C.Y., Y.Zhou, Y.D., M.F., C.Z., D.X., and Y.Zhu. performed positive selection analysis. Y.Zhou, Z.S., and G.Z. performed

brain/disease related analysis. G.Z., E.D.J., M.H.S, C.Y., Y.Zhou, S.M., L.B., J.Be., M.M.R., G.F., X.B., and Z.S. wrote the manuscript.

Competing interests The authors declare no competing interests.

Additional information

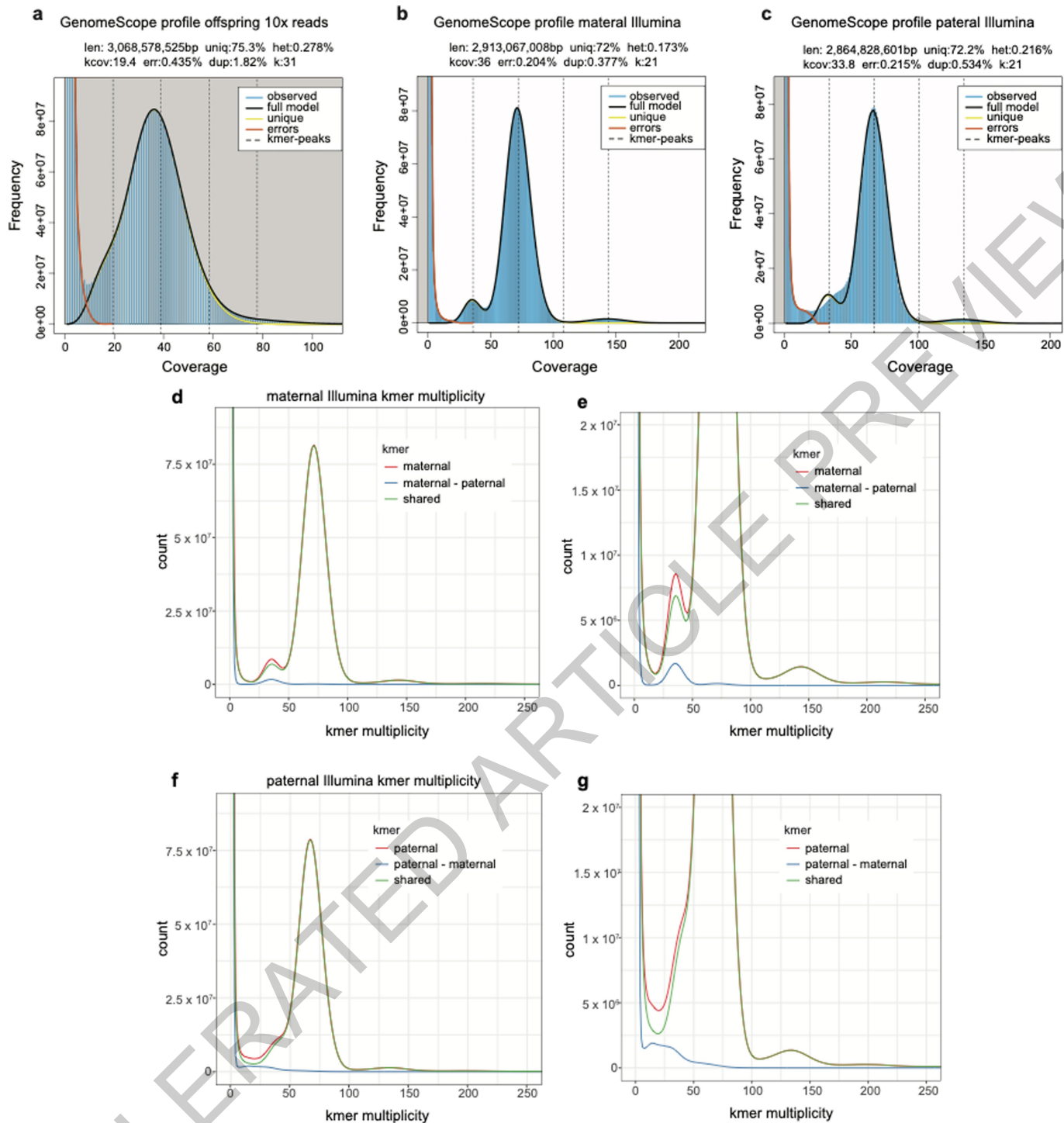
Supplementary information The online version contains supplementary material available at <https://doi.org/10.1038/s41586-021-03535-x>.

Correspondence and requests for materials should be addressed to G.Z.

Peer review information *Nature* thanks Joanna Malukiewicz, Vagheesh Narasimhan and the other, anonymous, reviewer(s) for their contribution to the peer review of this work.

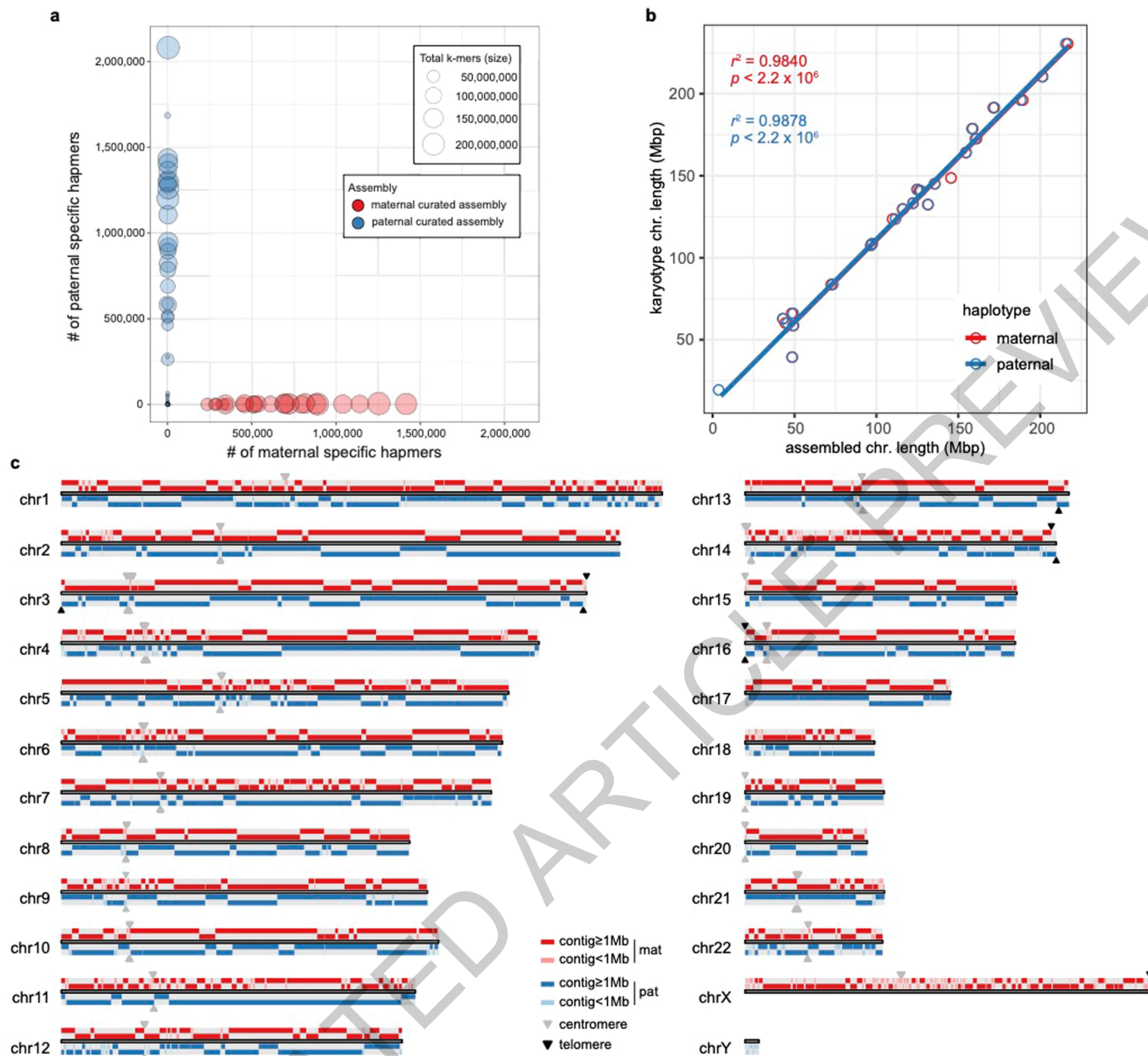
Reprints and permissions information is available at <http://www.nature.com/reprints>.

ACCELERATED ARTICLE PREVIEW



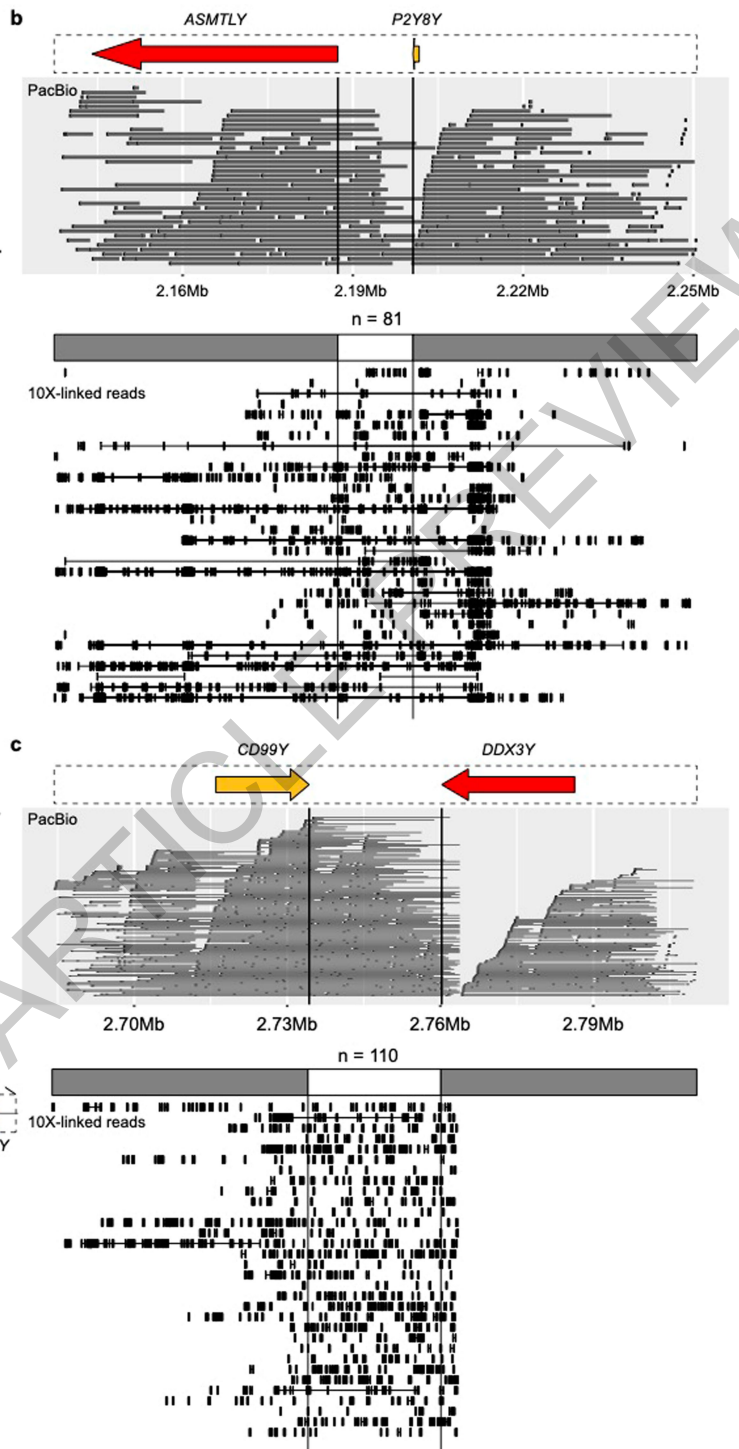
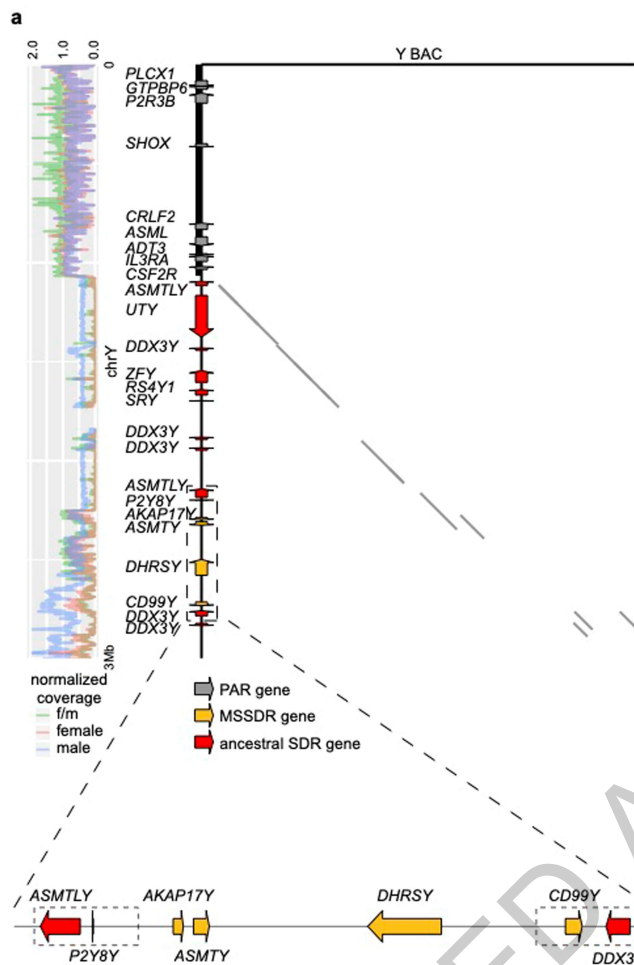
Extended Data Fig. 1 | GenomeScope analyses. **a**, GenomeScope (v1.0) profile for 31-mers collected from the F1 10x reads via meryl (following GEM barcode trimming). Heterozygosity estimated at a maximum 0.287%. Read error rate estimated at a maximum 0.435%. Genome haploid length estimated at max 3,068,578,525 bp, repeat length estimated at max 757,852,942 bp, and unique length estimated at a max 2,310,725,582 bp. GenomeScope profiles of the **b**, maternal and **c**, paternal 21-mers collected from the raw Illumina data; the observed paternal data does not fit GenomeScope's robust model (black line) for a diploid organism and exhibits higher overall heterozygosity than the

maternal data, at 0.216% compared to 0.173%. This supports a premise that the father's sequencing reads contain a level of chimerism, while the mother's reads contain negligible representation of alternative alleles, at most. Further analysis of the parental Illumina data shows that the k-mer multiplicity distribution varies greatly between the maternal and paternal sets. **d**, **e**, (zoomed in) The maternal k-mers show clear distributions with a distinct haploid peak at half coverage (~35x), whereas **f**, **g**, (zoomed in) the paternal k-mers show an irregular distribution with no clearly defined haploid peak. This further illustrates the paternal data exhibits a level of chimerism.



Extended Data Fig. 2 | Trio-based diploid genome assembly. **a**, Hapmer (haplotype-specific k-mer) blob plot of the curated marmoset assemblies; red: represents the maternal haplotype, and blue: the paternal haplotype. The size of each blob indicates the total number of k-mers counted in an individual scaffold and the position of each blob is plotted according to the number of contained maternal and paternal hapmers. We see maternal and paternal hapmers are highly phased, with some slight representation of paternal hapmers in several maternal scaffolds (those that do not lie directly on the x-axis). We can also see higher representation of paternal hapmers identified

within scaffolds of the paternal assembly than maternal hapmers identified in scaffolds of the maternal assembly. **b**, Correlation between the assembled chromosome sizes and the chromosome lengths estimated by karyotype image data. A total of 23 chromosomes are plotted and the coefficient of determination is calculated for each assembly. **c**, Schematic plot mapping the assembled maternal and paternal assigned contigs onto marmoset assembled chromosomes. Top: maternal alleles, bottom: paternal alleles. Contig sizes, centromeres, and telomeres are indicated.



Extended Data Fig. 3 | Confirmation of the MSSDR translocation in marmoset Y. **a**, Marmoset Y specific BAC reads were obtained from NCBI trace archive and constructed into a pseudo Y chromosome according to their position from Bellott et al. 2014²⁰. The linear alignment between mCalJac1's Y and Y BAC confirms the MSSDR translocation. The MSSDR translocation on Y is highlighted in yellow and the two regions spanning the breakpoints and its flanking 50kb are highlighted in dashed boxes. **b**, Region spanning *ASML* and

P2RY8Y is supported by PacBio reads and 10X linked-reads (only a proportion of them were shown). In the 10X linked-reads panel, each rectangle represents a read and each line represents a 10X DNA molecule. A total of 8110X linked DNA molecules support the linkage of *ASML* and *P2RY8Y*. **c**, Region spanning *CD99Y* and *DDX3Y* are supported by PacBio reads and 10X linked-reads (only a proportion of them shown). A total of 110 10X linked DNA molecules support the linkage of *CD99Y* and *DDX3Y*.

Reporting Summary

Nature Research wishes to improve the reproducibility of the work that we publish. This form provides structure for consistency and transparency in reporting. For further information on Nature Research policies, see our [Editorial Policies](#) and the [Editorial Policy Checklist](#).

Statistics

For all statistical analyses, confirm that the following items are present in the figure legend, table legend, main text, or Methods section.

- | n/a | Confirmed |
|-------------------------------------|--|
| <input type="checkbox"/> | <input checked="" type="checkbox"/> The exact sample size (n) for each experimental group/condition, given as a discrete number and unit of measurement |
| <input type="checkbox"/> | <input checked="" type="checkbox"/> A statement on whether measurements were taken from distinct samples or whether the same sample was measured repeatedly |
| <input type="checkbox"/> | <input checked="" type="checkbox"/> The statistical test(s) used AND whether they are one- or two-sided
<i>Only common tests should be described solely by name; describe more complex techniques in the Methods section.</i> |
| <input checked="" type="checkbox"/> | <input type="checkbox"/> A description of all covariates tested |
| <input type="checkbox"/> | <input checked="" type="checkbox"/> A description of any assumptions or corrections, such as tests of normality and adjustment for multiple comparisons |
| <input type="checkbox"/> | <input checked="" type="checkbox"/> A full description of the statistical parameters including central tendency (e.g. means) or other basic estimates (e.g. regression coefficient) AND variation (e.g. standard deviation) or associated estimates of uncertainty (e.g. confidence intervals) |
| <input type="checkbox"/> | <input checked="" type="checkbox"/> For null hypothesis testing, the test statistic (e.g. F , t , r) with confidence intervals, effect sizes, degrees of freedom and P value noted
<i>Give P values as exact values whenever suitable.</i> |
| <input checked="" type="checkbox"/> | <input type="checkbox"/> For Bayesian analysis, information on the choice of priors and Markov chain Monte Carlo settings |
| <input checked="" type="checkbox"/> | <input type="checkbox"/> For hierarchical and complex designs, identification of the appropriate level for tests and full reporting of outcomes |
| <input type="checkbox"/> | <input checked="" type="checkbox"/> Estimates of effect sizes (e.g. Cohen's d , Pearson's r), indicating how they were calculated |

Our web collection on [statistics for biologists](#) contains articles on many of the points above.

Software and code

Policy information about [availability of computer code](#)

Data collection

Data analysis

For manuscripts utilizing custom algorithms or software that are central to the research but not yet described in published literature, software must be made available to editors and reviewers. We strongly encourage code deposition in a community repository (e.g. GitHub). See the Nature Research [guidelines for submitting code & software](#) for further information.

Data

Policy information about [availability of data](#)

All manuscripts must include a [data availability statement](#). This statement should provide the following information, where applicable:

- Accession codes, unique identifiers, or web links for publicly available datasets
- A list of figures that have associated raw data
- A description of any restrictions on data availability

Raw sequencing data for the marmoset trio is available under the GenomeArk github (https://vgp.github.io/genomeark/Callithrix_jacchus/). Curatorial information and data mappings to maternal and paternal assemblies are available on the genome evaluation browser, gEVAL (https://vgp-geval.sanger.ac.uk/all_genomes.html). The maternal, paternal, and combined (paternal autosomes and Y chromosome + maternal X chromosome + mitochondrial) assemblies, as well as PacBio Iso-Seq data for annotation, are available under the NCBI BioProject PRJNA560230 (<http://www.ncbi.nlm.nih.gov/bioproject/PRJNA560230>). The genome assemblies have also been deposited at CNSA of CNGBdb with accession CNP0001310 and CNP0001311. Chimpanzee NGS reads are obtained from ERP002376. The human SNV data of HG00096 was obtained from <https://www.internationalgenome.org/>. Published marmoset genomes are obtained with accession code GCA_000004665.1, GCA_001269965.1, GCA_002754865.1, GCA_009663435.1, GCA_009811775.1. Genomes used in brain related genes study include: human (hg38), marmoset (mCalJac1), chimpanzee (Clint_PTRv2), rhesus macaque (rheMacS), Ma's night monkey (Anan_2.0), and Chinese tree shrew (TS_2.0). Genomes used in positive selection section include: cow, human, chimpanzee, mouse from Ensembl 98 and Chinese tree shrew (TS_2.0), Cebus capucinus (GCF_001604975.1), Saimiri boliviensis (GCF_000235385.1), Aotus nancymaae (GCF_000952055.2) from NCBI.

Field-specific reporting

Please select the one below that is the best fit for your research. If you are not sure, read the appropriate sections before making your selection.

Life sciences Behavioural & social sciences Ecological, evolutionary & environmental sciences

For a reference copy of the document with all sections, see [nature.com/documents/nr-reporting-summary-flat.pdf](https://www.nature.com/documents/nr-reporting-summary-flat.pdf)

Life sciences study design

All studies must disclose on these points even when the disclosure is negative.

Sample size	We aim to use parental SNV to determine and phase the two offspring haplotype genome, thus the sample size for genome sequencing is three. Bioinformatic analyses were performed with all available data.
Data exclusions	Sex chromosomes are excluded in genetic variation analysis. In PCR validation, we excluded SNPs located in repeat elements. Variations in chimeric regions were excluded. Various filters were applied at the potential Mendelian violation to reduce false-positive calls, especially at chimerism sites. The first filter was on the site and applied as follows: QD < 2.0, FS > 20.0, MQ < 40.0, MQRankSum < -2.0, MQRankSum > 4.0, ReadPosRankSum < -3.0, ReadPosRankSum > 3.0, SOR > 3.0. The second set of filters were applied to each individual: - a depth filter DP < 0.5 × individual average depth and DP > 2 × individual average (average depth offspring: 40.5X, father: 72.6X, and mother: 76.9X). This filter would remove any high coverage caused by mapping problems and low coverage sites that are more sensitive to false-positive calls. - a genotype quality filter GQ < 99 for at least one individual. This filter was set particularly high (generally GQ < 40 to 60 in other de novo studies) to avoid a maximum of chimerism sites in the father, as those sites tend to have a lower genotype quality due to the presence of multiple alleles. - an alternative allele filter AD > 0 allowed in the homozygous parents. Again, this filter was set stringent with no alternative allele allowed in any parents as most of the chimerism sites would present at least a few alternative alleles in the variant calling files. - an allelic balance filter AB < 0.3 and AB > 0.7 on the reads supporting the alternative allele in the heterozygous offspring. This filter would remove any potential sequencing errors in the offspring or chimerism cells as those should present a lower allelic balance (~10-20 %) than the real de novo mutations (~50 %). In positive selection gene analysis, to minimize effects of alignment, we filtered genes based on the condition of its positively selected sites following these criterions, 1) sites with gap number more than 2 were excluded; 2) sites with nonsynonymous substitutions larger than 2 were excluded; and 3) more complicated cases found manual checks. If one gene had no confident site, the gene would be removed.
Replication	Experiments performed in this study aim to validate the variation between the two alleles of the offspring, thus the experiments were performed based on the offspring DNA sample and replication is not applied in this study.
Randomization	Randomization for genome and transcriptome sequencing is not applied in this study. For SNV and indel PCR validation, variation sites were randomly selected by Linux command "sort -R".
Blinding	Blinding was not necessary for genome and transcriptome sequencing, as well as genetic variation PCR validation. The study aim to study the genetic difference inherent from parental genome, so only the F1 individual DNA sample is used for PCR validation.

Reporting for specific materials, systems and methods

We require information from authors about some types of materials, experimental systems and methods used in many studies. Here, indicate whether each material, system or method listed is relevant to your study. If you are not sure if a list item applies to your research, read the appropriate section before selecting a response.

Materials & experimental systems

n/a	Involvement	Included
<input checked="" type="checkbox"/>	<input type="checkbox"/>	Antibodies
<input checked="" type="checkbox"/>	<input type="checkbox"/>	Eukaryotic cell lines
<input checked="" type="checkbox"/>	<input type="checkbox"/>	Palaeontology and archaeology
<input type="checkbox"/>	<input checked="" type="checkbox"/>	Animals and other organisms
<input checked="" type="checkbox"/>	<input type="checkbox"/>	Human research participants
<input checked="" type="checkbox"/>	<input type="checkbox"/>	Clinical data
<input checked="" type="checkbox"/>	<input type="checkbox"/>	Dual use research of concern

Methods

n/a	Involvement	Included
<input checked="" type="checkbox"/>	<input type="checkbox"/>	ChIP-seq
<input checked="" type="checkbox"/>	<input type="checkbox"/>	Flow cytometry
<input checked="" type="checkbox"/>	<input type="checkbox"/>	MRI-based neuroimaging

Animals and other organisms

Policy information about [studies involving animals](#); [ARRIVE guidelines](#) recommended for reporting animal research

Laboratory animals	Species: <i>Callithrix jacchus</i> . No unique strain. Male and female animals used. Ages: mCalJac1 (M) = 3 months, mCalJac2 (M) = 3 years, mCalJac3 (F) = 3 years, mCalJac4 (M) = 1.5 years.
Wild animals	Study did not involve wild animals.
Field-collected samples	Study did not involve field-collected samples.
Ethics oversight	USDA, AAALAC, and The Rockefeller University IACUC

Note that full information on the approval of the study protocol must also be provided in the manuscript.